Convective instability of heat and mass transfer for laminar forced convection in the thermal entrance region of horizontal rectangular channels

J. N. Lin* and P. Y. Tzeng‡
Department of System Engineering* and Department of Aeronautical Engineering,‡
Chung-Cheng Institute of Technology, Tashi, Taiwan, Republic of China

F. C. Chou
Department of Mechanical Engineering, National Central University, Chung-Li, Taiwan, Republic of China

W. M. Yan
Department of Mechanical Engineering, Hua Fan Institute of Technology, Taipei, Taiwan, Republic of China

A numerical analysis is performed to investigate the onset of convective instability and latent heat transfer, in connection with the vaporization of a liquid-water film, for laminar forced convection in the thermal entrance region of horizontal rectangular ducts. Major dimensionless groups identified are aspect ratio γ, effective Rayleigh number Ra^+, Prandtl number Pr, and Schmidt number Sc. The effects of the changes of bottom wall temperature T_w, relative humidity of air ϕ, γ, and Ra^+ on the local Nusselt number Nu_z, Sherwood number Sh_z, and the onset point of convective instability are examined in detail. To understand the effects of the selection of different criteria on the onset point, two typical definitions are chosen: a 2 percent departure of Nu_z from that of Graetz theory and the local minimum Nu_z. Results show that the onset point, under the effects of the combined buoyancy forces of thermal and mass diffusion, is rather advanced compared with that under the effect of thermal buoyancy force only. Results also show that the convective instability is affected by changes of ϕ and T_w for fixed γ. Additionally, the influence of water evaporation along the wetted wall on the laminar mixed convection heat transfer in this study is also presented.

Keywords: convective instability; heat and mass transfer; thermal entrance region; latent heat transport

Introduction

The flow and heat transfer phenomena of laminar forced convection are significantly affected by buoyancy-induced secondary flow. Thus, the effect of buoyancy force on laminar forced convective flows with various geometrical shapes has been studied by many investigators in recent years. The buoyancy effect is particularly pronounced for horizontal ducts where it may act to enhance heat transfer and induce early transition to turbulence. The precursor to the effect is a convective instability that results in the development of longitudinal vortex rolls. Hence, to establish the existence of the buoyancy effect, conditions marking the onset of convective instability must be known. However, in practical applications the convective heat transfer is often accompanied by mass transfer. Noticeable examples include chemical distillation processes, design of heat exchangers, channel type solar energy collectors, and thermoprotection systems. Hence, the influence of combined buoyancy forces, due to the variations of temperature and concentration, on the onset of convective instability is relatively important.

A great many published works, both theoretical and experimental, have studied thermal buoyancy effects on laminar forced convection in the thermal entrance region of rectangular channels. Only those related to the present study are briefly reviewed here. A linear stability analysis is usually used to determine the onset of longitudinal vortex rolls between two horizontal parallel plates.[1,2] The buoyancy effects, under a large Prandtl number assumption, on laminar forced convection in the thermal entrance regions of horizontal channels were studied by Cheng and his coworkers.[3–5] Recently, the primitive variable method was used by Abou-Ellail and Morcos[6] and Incropera and his coworkers[7–9] to examine numerical buoyancy effects on the Graetz problem in horizontal entrance flows. By the vorticity-velocity calculation procedure, Chou and Hwang[10] carried out studies of laminar mixed convection heat transfer in a horizontal square entrance flow with a constant wall heat flux. Lin *et al.*[11] performed a theoretical prediction of the onset of thermal instability in the thermal entrance region of a horizontal rectangular channel.

Address reprint requests to Dr. Chou at the Department of Mechanical Engineering, National Central University, Chung-Li, Taiwan 320, Republic of China.

Received 15 February 1991; accepted 9 September 1991

To verify the predictions, several investigators[12–14] visualized air flow in horizontal parallel-plate channels heated from below. A single stream of dye was injected along the midline of the bottom plate and a side view was used to determine the longitudinal station at which the buoyancy force caused the dye to ascend or descend from the plate. Kamotani and Ostrach[15] also performed experiments for air flow in thermally developing channel flow to determine the onset of the convective instability by detecting small spanwise temperature variations. It is noteworthy that the measured values of the critical Rayleigh number exceeded predictions by more than an order of magnitude. A similar experimental study for water flow in a horizontal duct was done by Incropera *et al.*[16] Correlations for the critical Rayleigh number, which are determined by flow visualization and occurrence of minimum local Nusselt number, are found to be a function of Graetz number.

The effects of combined buoyancy forces of heat and mass diffusion on convective heat transfer have been well examined. Sound-Algekar and Ganesan[17] investigated combined heat and mass transfer from a vertical plate in natural convection flows. Natural convection in a vertical plate channel with reversed buoyancy forces was studied by Lee *et al.*[18] In a vertical open tube, the effects of the coupled buoyancy forces of thermal and mass diffusion on natural convection flows were investigated by Chang *et al.*[19] As mixed convection heat and mass transfer characteristics are involved, Santarelli and Foraboschi[20] examined the buoyancy effects on laminar forced convection flow undergoing a chemical reaction. Recently, the characteristics of heat and mass transfer in a vertical wetted-wall channel were studied by Lin *et al.*[21] and Yan *et al.*[22] In their analyses, they found that the heat transfer along the wetted wall is dominated by the transport of latent heat in association with film evaporation.

In spite of its importance in engineering applications, convective instability under the combined effects of thermal and mass diffusion in the thermal entrance region of horizontal rectangular channel flows has not yet been evaluated. This motivates the present study. Instead of the conventional linear stability theory, the vorticity-velocity formulation of the Navier-Stokes equations together with the energy and concentration equations is used to investigate the convective instability. In this work, the geometry of the system under consideration, as schematically shown in Figure 1, is a rectangular duct whose bottom surface is wetted by an extremely thin liquid film and maintained at a uniform temperature, T_w, that is higher than the ambient temperature, T_0. The other walls are taken to be adiabatic and semipermeable.

In the present study, a 2 percent deviation of local Nusselt number from the value for pure forced convection[5] and the local minimum Nu_z[8] are used as the two criteria for the prediction of the onset of convective instability. The specific effects of γ, T_w, ϕ, and Ra^+ on the instability are examined in detail. Also, the effects of Ra^+ on the mixed convection heat

Notation

A	Cross-sectional area of a horizontal rectangular channel
a, b	Width and height of a rectangular channel, respectively
C	Mass fraction of water vapor
c	Dimensionless quantity for C, $(C - C_0)/(C_w - C_0)$
D	Mass diffusivity
D_e	Equivalent hydraulic diameter, $4A/S$
g	Gravitational acceleration
Gr_t	Heat transfer Grashof number, $g\beta(T_w - T_0)D_e^3/\nu^2$
Gr_m	Mass transfer Grashof number, $g(M_a/M_v - 1)(C_w - C_0)D_e^3/\nu^2$
h	Local heat transfer coefficient
h_m	Local mass transfer coefficient
k	Thermal conductivity
M	Number of finite difference divisions in X-direction
M_a	Molecular weight of air
M_v	Molecular weight of water vapor
N	Number of finite difference divisions in Y-direction
n	Outward normal direction to the wall
Nu_l	Local Nusselt number (latent heat)
Nu_s	Local Nusselt number (sensible heat)
Nu_z	Overall local Nusselt number ($= Nu_s + Nu_l$)
P	Mixture pressure
$\bar{P}$	Cross-sectional mean pressure
$\bar{p}$	Dimensionless quantity for $\bar{P}$
P'	Perturbation term about the mean pressure $\bar{P}$
p'	Dimensionless quantity for P'
Pr	Prandtl number, ν/α
Ra^+	Effective Rayleigh number, ($= PrGr_t + ScGr_m$)
Ra_c	Critical Rayleigh number, $Ra_c = [(1 + 1/\gamma)^3/8]R_a^+$
Re	Reynolds number, $\bar{W}_0 D_e/\nu$
S	Circumference of cross section
S^*	Parameter, $\rho D h_{fg}(C_w - C_0)/[k(T_w - T_0)]$
Sc	Schmidt number, ν/D
Sh_z	Local Sherwood number, $Sc(1 - C_w)(\partial c_b/\partial z)/(1 - C_b)$
T	Temperature
T_0	Uniform fluid temperature at entrance
T_w	Bottom wall temperature
U, V, W	Velocity components in X-, Y-, Z-directions, respectively
u, v, w	Dimensionless quantities for U, V, and W, respectively
v_e	Dimensionless interfacial velocity of mixture
w	Dimensionless quantitites for W
W_0	Fully developed axial velocity before thermal entrance
$\bar{W}_0$	Mean quantity for W_0
X, Y, Z	Rectangular coordinates
x, y, z	Dimensionless rectangular coordinates

Greek symbols

α	Thermal diffusivity
β	Coefficient of thermal expansion
γ	Aspect ratio of a rectangular channel, a/b
θ	Dimensionless temperature, $(T - T_0)/(T_w - T_0)$
ν	Kinematic viscosity
ξ	Dimensionless vorticity in axial direction
ρ	Density
ϕ	Relative humidity of air in the ambient condition

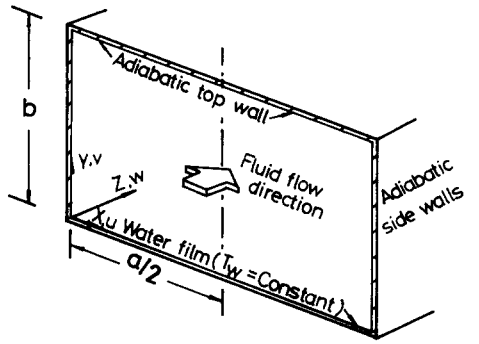

Figure 1 Flow in a horizontal rectangular channel

and mass transfer with different γ in the flow are considered. Finally, a comparison between the results based on the two criteria under the effects of combined buoyancy forces of thermal and mass diffusion are made to study the influence of the choice of criterion.

Theoretical analysis

In this preliminary study of mixed convective heat and mass transfer in the thermal entrance region of a horizontal rectangular channel, the liquid water film on the bottom wall is considered to be so thin that it can be treated as a boundary condition for heat and mass transfer, i.e., the liquid film is stationary and maintained at the same temperature as that of the bottom surface, T_w. In reality, the liquid film is finite in thickness. It may move forward or backward along the bottom wall and result in a liquid–gas interface of complicated shape. This complicated interfacial phenomenon is formidable to study without the help of experiments. However, the validity of the assumption that the influence of the liquid film with finite thickness on the heat and mass transfer in the gas stream is insignificant for a small liquid mass flow rate was well documented by Yan and Lin.[23] Therefore, the assumption of zero film thickness is appropriate in the present study.

The horizontal channel flow, depicted in Figure 1, is three dimensional and characterized by velocity components u, v, and w in the spanwise X-, vertical Y-, and longitudinal Z-directions. A fully developed axial velocity profile is imposed at the entrance ($z/\mathrm{Pr} = 0$) and constant wall temperature and concentration are imposed on the bottom surface at $z/\mathrm{Pr} > 0$. To facilitate the analysis, an order of magnitude analysis is used that simplifies the governing equations by neglecting the axial diffusions of momentum, heat, and mass.[7,9,10] In addition, the thermophysical properties of the mixture are assumed to be constant and are evaluated by the one-third rule,[24] i.e., $T^* = T_w + (T_0 - T_w)/3$ and $C^* = C_w + (C_0 - C_w)/3$, where T^* and C^* are the temperature and mass fraction of water vapor at reference state, respectively. The detailed evaluation of the properties is performed by Fujii *et al.*[25] and Yan.[26] The formulation of the problem based on the Boussinesq approximation is briefly presented, with the details being given in a previous study.[10] Referring to the coordinate system (Figure 1) and introducing the following dimensionless variables and parameters

$$x = X/[D_e], \quad y = Y/[D_e], \quad z = Z/[\mathrm{Re}\, D_e]$$
$$u = UD_e/v, \quad v = VD_e/v, \quad w = W/[\bar{W}_0],$$
$$\theta = (T - T_0)/[T_w - T_0], \quad c = (C - C_0)/[C_w - C_0],$$
$$\bar{p} = \bar{P}/[\rho \bar{W}_0^2], \quad p = P/[P_c], \quad P_c = \rho v^2/[D_e^2],$$
$$\mathrm{Re} = \bar{W}_0 D_e/v, \quad \mathrm{Pr} = v/\alpha, \quad \mathrm{Sc} = v/D, \tag{1}$$

$$\mathrm{Gr}_t = g\beta(T_w - T_0)D_e^3/v^2,$$
$$\mathrm{Gr}_m = g(M_a/M_v - 1)(C_w - C_0)D_e^3/v^2$$

where $D_e = 4A/S$, and $\bar{P} = \bar{P}(Z)$ is the cross-section mean pressure driving the main flow, and $P' = P'(X, Y, Z)$ is the perturbation term about the mean, which drives the cross-stream flows. By introducing a vorticity function in the axial direction, $\xi = \partial u/\partial y - \partial v/\partial x$, the following dimensionless governing equations including the vorticity transport equation can be obtained:

$$\nabla^2 u = \frac{\partial \xi}{\partial y} - \frac{\partial^2 w}{\partial x\, \partial z} \tag{2}$$

$$\nabla^2 v = -\frac{\partial \xi}{\partial x} - \frac{\partial^2 w}{\partial y\, \partial z} \tag{3}$$

$$u\frac{\partial \xi}{\partial x} + v\frac{\partial \xi}{\partial y} + w\frac{\partial \xi}{\partial z} + \xi\left(\frac{\partial u}{\partial x} + \frac{\partial v}{\partial y}\right) + \left(\frac{\partial w}{\partial y}\frac{\partial u}{\partial z} - \frac{\partial w}{\partial x}\frac{\partial v}{\partial z}\right) = \left(\frac{\partial^2 \xi}{\partial x^2} + \frac{\partial^2 \xi}{\partial y^2}\right) - \left(\mathrm{Gr}_t \frac{\partial \theta}{\partial x} + \mathrm{Gr}_m \frac{\partial c}{\partial x}\right) \tag{4}$$

$$u\frac{\partial w}{\partial x} + v\frac{\partial w}{\partial y} + w\frac{\partial w}{\partial z} = -\frac{\partial \bar{p}}{\partial z} + \left(\frac{\partial^2 w}{\partial x^2} + \frac{\partial^2 w}{\partial y^2}\right) \tag{5}$$

$$u\frac{\partial \theta}{\partial x} + v\frac{\partial \theta}{\partial y} + w\frac{\partial \theta}{\partial z} = \frac{1}{\mathrm{Pr}}\left(\frac{\partial^2 \theta}{\partial x^2} + \frac{\partial^2 \theta}{\partial y^2}\right) \tag{6}$$

$$u\frac{\partial c}{\partial x} + v\frac{\partial c}{\partial y} + w\frac{\partial c}{\partial z} = \frac{1}{\mathrm{Sc}}\left(\frac{\partial^2 c}{\partial x^2} + \frac{\partial^2 c}{\partial y^2}\right) \tag{7}$$

where $\nabla^2 = \partial^2/\partial x^2 + \partial^2/\partial y^2$.

Because of vertical symmetry, only half of the channel region is considered. The governing equations are subjected to the following boundary conditions:

$u = v = w = 0, \quad \partial\theta/\partial n = \partial c/\partial n = 0$
at the top and side walls
$(y = (\gamma + 1)/2\gamma, \quad x = 0, \quad (\gamma + 1)/2)$

$u = w = 0, \quad v = v_e, \theta = c = 1$
at the bottom wall $(y = 0)$ (8)

$u = \partial v/\partial x = \partial w/\partial x = \partial\theta/\partial x = \partial c/\partial x = 0$
at the symmetric plane
$(x = (\gamma + 1)/4)$

$u = v = \xi = \theta = c = 0$
at the entrance $(z/\mathrm{Pr} = 0)$

Since the air–water interface is semipermeable (the solubility of air in water is negligibly small and air velocity in the vertical direction is zero at the interface), the evaporating velocity of the mixture along the wetted wall is evaluated by the following equation[27]:

$$v_e = -(C_w - C_0)(\partial c/\partial y)/[\mathrm{Sc}(1 - C_w)] \tag{9}$$

According to Dalton's law and the state equation of an ideal gas mixture, the interfacial mass fraction of water vapor can be individually calculated by

$$C_w = P_w M_v/[P_w M_v + (P - P_w)M_a] \tag{10}$$

where P_w is the saturated vapor pressure of water at the bottom wall. The overall mass flow rate must be balanced at every axial location in the channel:

$$\int_0^{(1+\gamma)/2\gamma}\int_0^{(1+\gamma)/4} w\, dx\, dy = 1/2 + \int_0^z \int_0^{(1+\gamma)/4} v_e\, dx\, dz \tag{11}$$

This equation is employed to deduce the pressure gradient in Equation 5.

Having obtained the developing velocity, temperature, and concentration fields, the computations may be made of local Nusselt number and Sherwood numbers, which are of practical interest. The total heat flux from the bottom wall can be expressed as[28]

$$q_i'' = q_s'' + q_l'' = -k(\partial T/\partial Y) - \rho D h_{fg}(\partial C/\partial Y)/(1 - C_w) \quad (12)$$

where q_i'', q_s'', and q_l'' denote the interfacial heat flux, sensible, and latent heat fluxes, respectively. The local Nusselt number defined by

$$\mathrm{Nu}_z = q_i'' D_e/[k(T_w - T_b)] \quad (13)$$

can be written as

$$\mathrm{Nu}_z = \mathrm{Nu}_s + \mathrm{Nu}_l \quad (14)$$

where Nu_s and Nu_l are obtained by considering the overall energy balance for axial length dz.

$$\mathrm{Nu}_s = Pr(\partial\theta_b/\partial z)/(1 - \theta_b) \quad (15a)$$

$$\mathrm{Nu}_l = S^*\mathrm{Sc}(\partial c_b/\partial z)/(1 - \theta_b) \quad (15b)$$

$$S^* = \rho D h_{fg}(C_w - C_0)/[k(T_w - T_0)] \quad (16)$$

where S^* signifies the importance of the energy transport through species diffusion relative to that through thermal diffusion. For a low mass transfer rate at the interface, a mass transfer coefficient h_m based on an overall mass balance is defined by

$$\rho h_m a(\Delta Z)\cdot(C_w - C_0) = \rho A W\, \Delta C(1 - C_w) \quad (17)$$

The local Sherwood number then becomes

$$\mathrm{Sh}_z = h_m D_e/D = \mathrm{Sc}(1 - C_w)(\partial c_b/\partial z)/(1 - C_b) \quad (18)$$

Solution methods

Because of a step change in wall temperature and concentration being imposed on the bottom surface, a numerical instability arises in the parabolic energy and concentration Equations 6 and 7, particularly near the entrance region ($z/\mathrm{Pr} < 10^{-3}$). This leads to a serious restriction on the axial step size Δz. After considerable numerical experiment, an axial step size Δz ranging from 7×10^{-6} near the entrance to 3×10^{-4} near the fully developed region were found to be satisfactory. The cross-sectional mesh size ($M \times N$) of 16×32 (for $\gamma = 2$) and 40×16 (for $\gamma = 10$) were used. On average the computing times required for each step is about 2.2 (for $\gamma = 2$) and 3.5 (for $\gamma = 10$) CPU seconds on a VAX-8650 computer. The total number of axial steps is 1,400 ($z/\mathrm{Pr} = 0.3$).

Since the flow under consideration is of a boundary layer type in the z-direction, the solution for Equations 2–7 can be marched in the downstream direction. Briefly, the numerical solution to the set of simultaneous equations subject to the boundary conditions 8 consists of the following main steps:

(1) The axial velocity at the entrance ($z/\mathrm{Pr} = 0$), constrained to $\bar{W}_0 = 1$, is solved independently using the successive overrelaxation method.

(2) The initial values for u, v, θ, and c are assigned zero at the entrance, $z/\mathrm{Pr} = 0$.

(3) For any axial location, with known values of u and v and guessed ($d\bar{p}/dz$), the axial velocity w at the current axial location is obtained from Equation 5. The convergence of w can be tested by checking the satisfaction of the overall conservation of mass (Equation 11). When the criterion

$$\left| \int_0^{(\gamma+1)/2\gamma} \int_0^{(\gamma+1)/4} w\, dx\, dy - \left(1/2 + \int_0^z \int_0^{(\gamma+1)/4} v_e\, dx\, dz\right) \right| < 10^{-5}$$

is reached, then the values of $\partial w/\partial x$ and $\partial w/\partial y$ can be computed at each grid point.

(4) With the results of $\partial w/\partial x$ and $\partial w/\partial y$ obtained from step 3, the values of $\partial u/\partial z$ and $\partial v/\partial z$ are computed by using a two-point backward difference. With the known values of u, v, and w, the Equations 4, 6, and 7 for ξ, θ, and c subject to the boundary conditions are solved by the Du Fort-Frankel method.[29]

(5) The elliptic-type equations, Equations 2 and 3, are solved for u and v by iteration. During the iteration process, the values of vorticity on the boundaries are evaluated simultaneously with u and v in the interior region.[10]

(6) Steps 3 and 4 must be repeated until the following convergence criteria are satisfied for u and v:

$$\varepsilon = \sum |(u_{i,j}^{(n+1)} - u_{i,j}^{(n)})/u_{i,j}^{(n+1)}/(M \times N)| < 5 \times 10^{-5}$$

$$\varepsilon = \sum |(v_{i,j}^{(n+1)} - v_{i,j}^{(n)})/v_{i,j}^{(n+1)}/(M \times N)| < 5 \times 10^{-5}$$

where M and N are the number of divisions in the x- and y-directions, respectively.

(7) Procedures 3–7 are applied successively to every axial location from the entrance to the downstream region.

To obtain enhanced accuracy or avoid the instability of numerical computation in the near entrance region, grids are chosen to be nonuniform in the axial direction to account for the significant variations of velocity, temperature, and concentration in the entrance region. The first axial interval Δz is taken to be 7×10^{-6} and the subsequent interval is enlarged by 0.4 percent over the prior value, i.e., $\Delta z_i = 1.004\Delta z_{i-1}$. A numerical experiment for cases 1 and 4 (Tables 1 and 2) with fixed T_w (= 40°C), ϕ (= 50 percent), Pr, and Sc was made to determine the grid sizes required for acceptable accuracy. An oscillatory behavior in local Nusselt number appears in the range of $z/\mathrm{Pr} < 10^{-3}$ when the Du Fort-Frankel method is used, but this undesired instability can be precluded by using

Table 1 Numerical experiment on mesh size ($M \times N$) and axial step size (Δz) for case 1 with $\gamma = 2$, Pr = 0.7, Sc = 0.6, ϕ = 50 percent and $\mathrm{Ra}^+ = 8.68 \times 10^4$

$M \times N$ (Δz)	Nu_z, z/Pr 0.001	0.005	0.010	0.200	0.300
16×32 ($7 \times 10^{-6} \sim 3 \times 10^{-4}$)	65.987	39.863	35.395	31.725	25.274
16×32 ($1.4 \times 10^{-5} \sim 3 \times 10^{-4}$)	66.872	39.783	35.407	31.723	25.415
20×40 ($7 \times 10^{-6} \sim 3 \times 10^{-4}$)	66.329	40.144	36.244	31.835	25.299

Table 2 Numerical experiment on mesh size ($M \times N$) and axial step size (Δz) for case 4 with $\gamma = 10$, Pr = 0.7, Sc = 0.6, $\phi = 50$ percent and $Ra^+ = 1.12 \times 10^5$

$M \times N$ (Δz)	Nu_z z/Pr 0.001	0.005	0.010	0.200	0.300
40 × 16 ($7 \times 10^{-6} \sim 3 \times 10^{-4}$)	72.998	44.297	37.490	28.453	19.862
40 × 16 ($1.4 \times 10^{-5} \sim 3 \times 10^{-4}$)	73.086	44.187	37.563	28.330	19.931
50 × 20 ($7 \times 10^{-6} \sim 3 \times 10^{-4}$)	73.352	44.414	37.762	28.456	19.807

Table 3 Values of major parameters for typical cases under fixed ambient temperature $T_0 = 20°C$

Case	γ	T_w (°C)	ϕ (%)	Pr	Sc	a (cm)	Ra^+	S^*
1	2	40	50	0.70	0.59	5	8.68×10^4	5.391
2	2	60	50	0.70	0.58	4	8.87×10^4	8.062
3	2	40	90	0.70	0.59	5	8.37×10^4	4.589
4	10	40	50	0.70	0.59	20	1.12×10^5	5.391
5	10	60	50	0.70	0.58	19	1.92×10^5	8.062
6	10	40	90	0.70	0.59	20	1.09×10^5	4.589

a simple forward difference for axial derivative $\partial\theta/\partial z$ and $\partial c/\partial z$ as suggested by Ou and Cheng.[29] As shown in Tables 1 and 2, the maximum deviation in Nu_z calculated is always less than 2.5 percent for case 1 and 1.0 percent for case 4. These indicate that the size arrangements, $M \times N(\Delta z) = 16 \times 32$ ($7 \times 10^{-6} \sim 3 \times 10^{-4}$) and $M \times N(\Delta z) = 40 \times 16$ ($7 \times 10^{-6} \sim 3 \times 10^{-4}$) are suitable for cases 1 and 4, respectively.

Results and discussion

The values of the nondimensional groups, i.e., Pr, Sc, Gr_t, Gr_m, and Ra^+ ($= PrGr_t + ScGr_m$), appearing in the analysis cannot all be arbitrarily assigned. In fact, they are interdependent for a given mixture under certain specified conditions. To be physically meaningful, the wall temperature T_w, the relative humidity of the ambient air ϕ, and hydraulic diameter D_e are here chosen as the independent parameters. In order to study the effects of T_w, ϕ, and γ on the onset of convective instability of heat and mass transfer, six cases shown in Table 3 are selected for the computation. Among these, the cases 1 and 4 are chosen as two typical cases for $\gamma = 2$ and $\gamma = 10$ to evaluate the influences of various Ra^+ and γ on the local Nusselt and Sherwood numbers.

The heat transfer characteristics in the thermal entrance region of rectangular channels are usually presented in terms of the spanwise local Nusselt number Nu_z at each axial position. Figures 2 and 3 show the distributions of Nu_z ($= Ns_s + Nu_t$) versus streamwise distance z/Pr, with Ra^+ as parameter for cases 1 ($\gamma = 2$) and 4 ($\gamma = 10$), respectively. The results disclose that the combined buoyancy effects can be neglected when $Ra^+ < 1.91 \times 10^3$ (case 1) and $Ra^+ < 1.75 \times 10^3$ (case 4). As Ra^+ increases, the convective instability occurs at shorter streamwise locations. It is worth noting that, after reaching the minimum value of Nu_z, subsequent oscillations occur with downstream distance when $Ra^+ > 4.46 \times 10^4$ (case 1) and $Ra^+ > 1.12 \times 10^5$ (case 4). The results then gradually approach an asymptotic situation. This confirms that the mixed convection flow becomes unstable if Ra^+ is high enough.[7] The

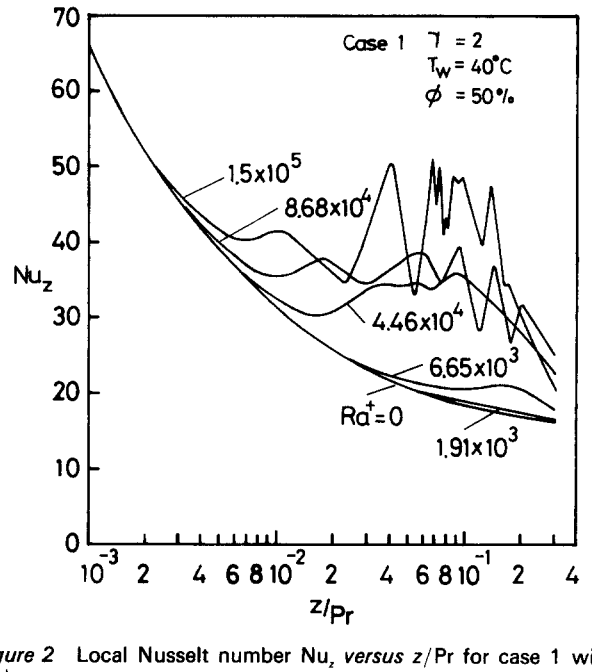

Figure 2 Local Nusselt number Nu_z *versus* z/Pr for case 1 with Ra^+ as parameter

minimum in the Nu_z distribution and the subsequent oscillatory phenomenon are also found in results for mixed convection heat transfer in a horizontal rectangular duct.[3,9] It is noticeable that the results of case 1 always show a more unstable heat transfer than those of case 4. This phenomenon is due to the side wall effects, which are more pronounced when the aspect ratio is small. The side walls induce a strong secondary flow in the region near them[5,11] and make the onset of instability occur earlier.

To understand the relative contributions of heat transfer through sensible and latent heat exchanges in the flow, the heat transfer by sensible heat exchange is illustrated in Figure 4 for case 1. Although the distributive trend of Nu_s is nearly the same

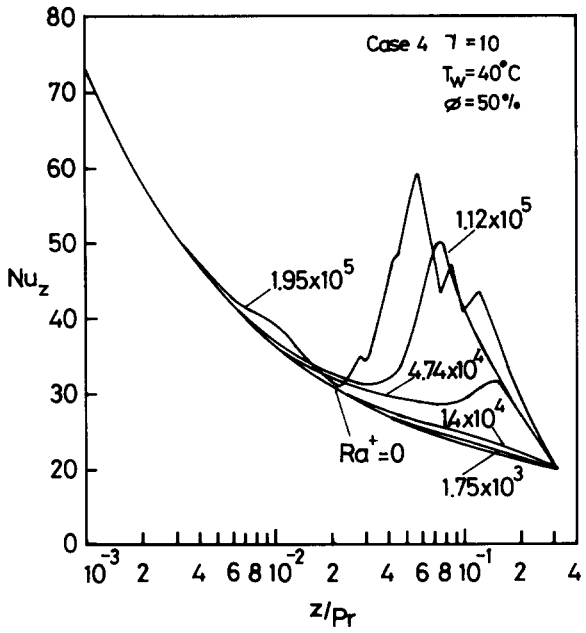

Figure 3 Local Nusselt number Nu_z *versus* z/Pr for case 4 with Ra^+ as parameter

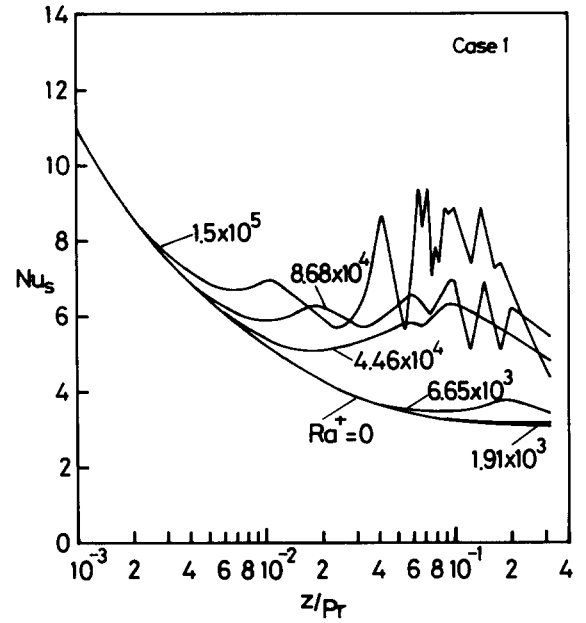

Figure 4 Local sensible heat Nusselt number Nu_s *versus* z/Pr for case 1 with Ra^+ as parameter

as that of Nu_z (Figure 2), the value of Nu_z is on average six times larger than that of Nu_s. This implies that the heat exchange along the wetted wall is dominated by the latent heat transfer in conjunction with the film vaporization. In case 4, the flow with large γ ($= 10$) also shows a significantly higher value of Nu_z than that of Nu_s (not shown).

The variations of local Sherwood number Sh_z versus z/Pr with Ra^+ as parameter for cases 1 and 4 are shown in Figures 5 and 6, respectively. As with the results of Nu_z (Figures 2 and 3), the effect of buoyancy on Sh_z is insignificant when $Ra^+ < 1.91 \times 10^3$ for case 1 and $Ra^+ < 1.75 \times 10^3$ for case 4. Comparing the corresponding predictions for Sh_z and Nu_s, it is observed that the variations in Sh_z (case 1) are like those of Nu_s, i.e., the values of Sh_z are only slightly smaller than those of Nu_s. This is attributed to the fact that the thermal boundary layer develops almost at the same rate as the concentration boundary layer because of the air–water mixture considered ($Pr = 0.7$ and $Sc = 0.6$). As to the effects of the change in γ on the distribution of Sh_z, Figure 6 reveals that the value of Sh_z for large γ is certainly higher. In addition, the flow is more stable for the system with larger aspect ratio owing to the weaker side wall effects.

Within the knowledge of the authors, there has not been any prior experimental work on laminar forced convection under the effects of the combined buoyancy effects of thermal and mass diffusion in the thermal entrance region of a geometry of

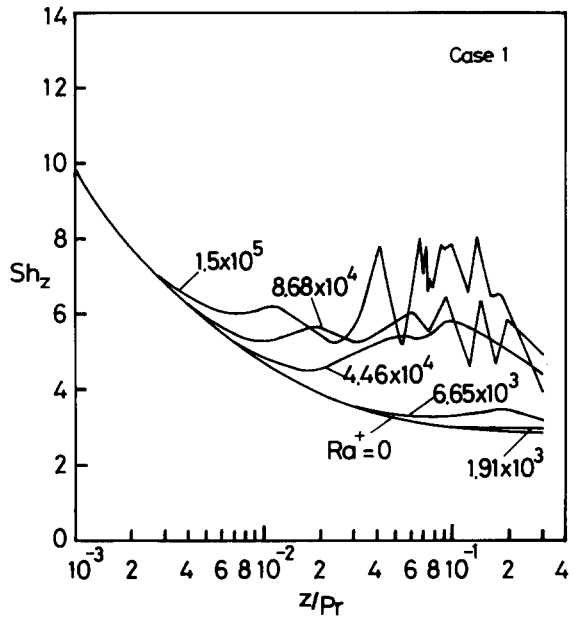

Figure 5 Local Sherwood number Sh_z *versus* z/Pr for case 1 with Ra^+ as parameter

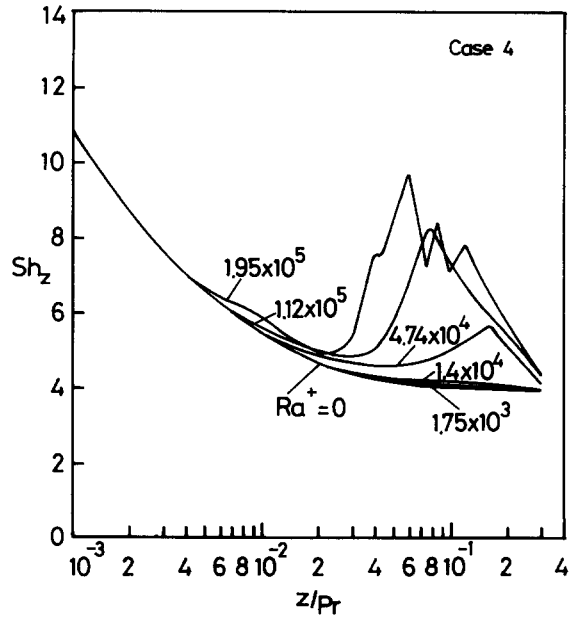

Figure 6 Local Sherwood number Sh_z *versus* z/Pr for case 4 with Ra^+ as parameter

this type. Concerning the present problem, the only available experimental results[13,15] were for the onset of convective instability under the thermal buoyancy effect condition. The experimental results of Hwang and Liu[13] and Kamotani and Ostrach[15] correspond to air flow in the thermal entrance region of horizontal parallel plate channels heated from below and isothermally cooled at the top plates with aspect ratios of approximately 15 and 17, respectively. The comparison of the present numerical results with others[13,15] for the instability in the horizontal rectangular channel is shown in Figures 7 and 8. To facilitate the comparison, the numerical results of this work were converted from an effective Rayleigh number Ra^+ based on equivalent hydraulic diameter and axial distance (z/Pr) to a critical Rayleigh number Ra_c based on the height (b) of the channel and axial distance z_c.

$$Ra_c = [(1 + 1/\gamma)^3/8]Ra^+ \tag{19}$$

$$z_c = [2/(1 + 1/\gamma)](z/Pr) \tag{20}$$

As shown in Figure 7a, under only thermal buoyancy effects (without mass diffusion), the predicted onset point of the convective instability based on the 2 percent deviation from the Graetz theory (also used by Ou *et al.*[5]) reveals a good agreement with the previous experimental results under a large aspect ratio condition, especially, when $Ra_c > 1.5 \times 10^4$. To examine the effects of mass diffusion on the onset of instability, the numerical results under the coupled buoyancy effects of thermal and mass diffusion are shown in Figure 7a for the two typical cases, 1 and 4. It is found that the point of onset advances when mass diffusion is involved in the thermal entrance flow. This indicates that the existence of the film evaporation results in an additional buoyancy force of mass diffusion and offers a more effective buoyancy effect.

To ascertain the effects of the bottom surface temperature T_w on the convective instability, it is of interest to compare the results for the system with different T_w. As shown in Figure 7b, the onset of convective instability is slightly earlier as T_w becomes large for both small and large aspect ratios. This is ascribed to a larger blowing effect (i.e., film evaporation ratio) for higher T_w. But the discrepancy decreases with the increase in Ra_c.

Figure 7c shows the effects of the relative humidity, ϕ, on the onset of convective instability. The result shows that under fixed T_w the onset point with higher ϕ (= 90 percent) slightly lags behind that of lower ϕ (= 50 percent). This is due to the smaller blowing effect for the system with higher ϕ. Therefore, the system is slightly more stable for higher ϕ. In the separate computation it is also found that the influence of ϕ on the onset of convective instability is insignificant.

The effects of the alternative criterion, based on the location of local minimum Nu_z, on the numerical prediction is also considered for comparison. The sharp decline of Nusselt number in the entrance region for the Graetz theory ($Ra^+ = 0$) is very well known. However, as the flow goes downstream, the influence of buoyancy increases. Eventually, the two effects

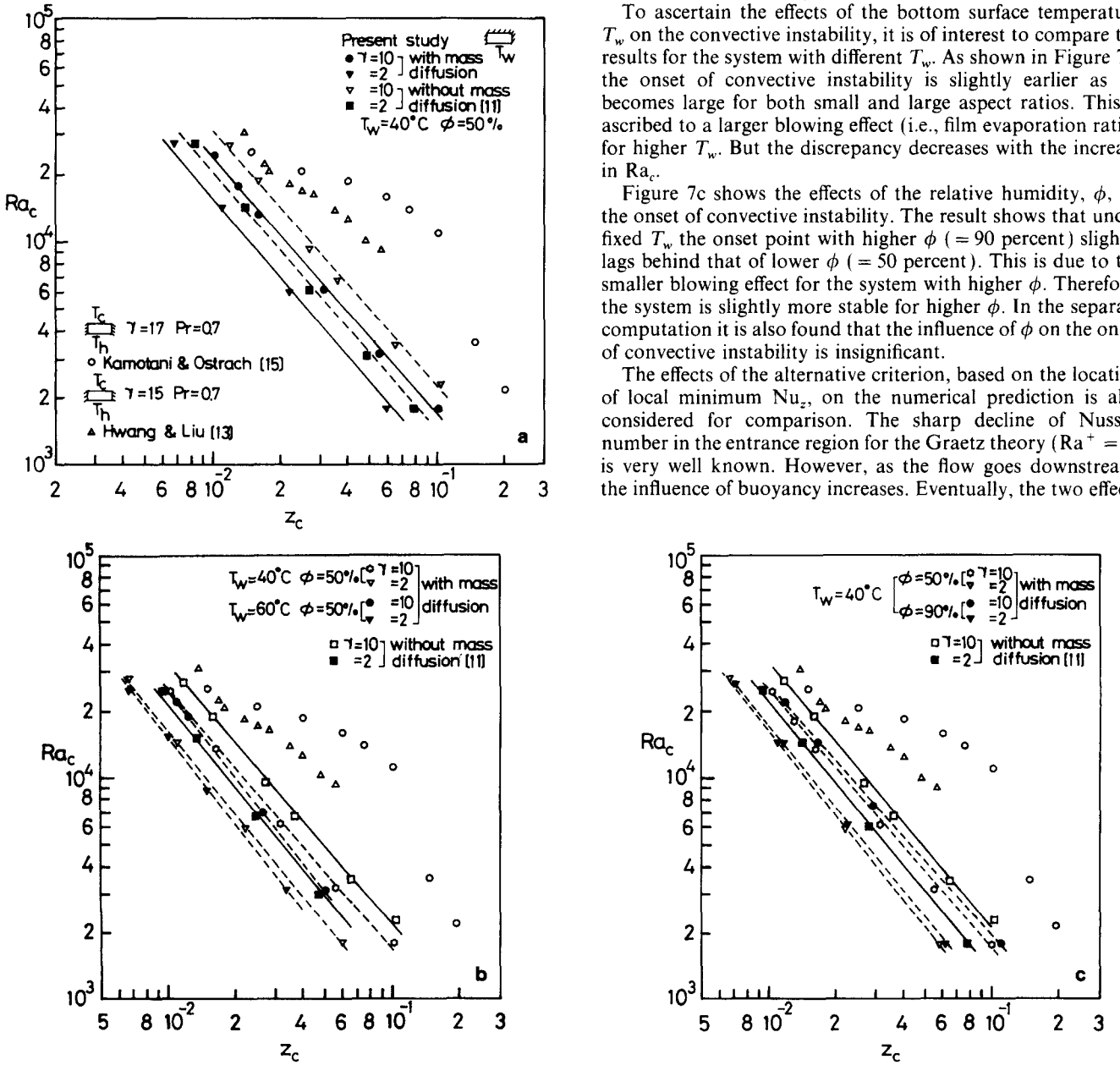

Figure 7 Comparison of the predictions of onset point based on a 2 percent departure among those with mass diffusion, without mass diffusion and previous experimental results (without mass diffusion) for (a) $T_w = 40°C$ and $\phi = 50$ percent; (b) $T_w = 60°C$ and $\phi = 50$ percent; (c) $T_w = 40°C$ and $\phi = 90$ percent

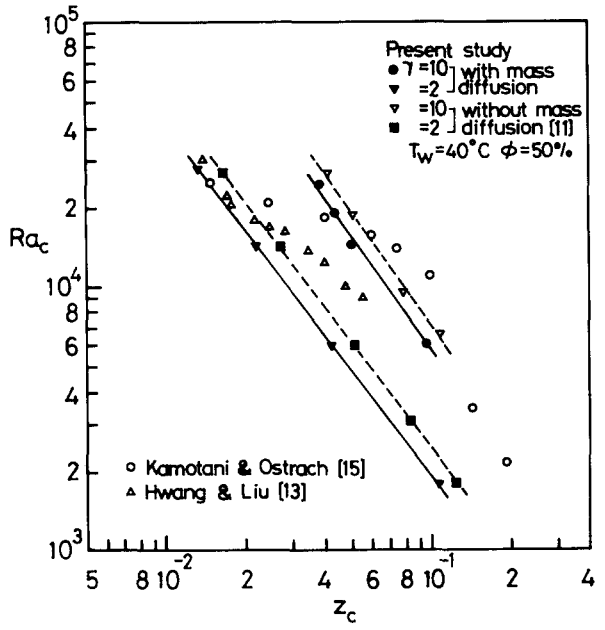

Figure 8 Comparison of the predictions of onset point based on the minimum Nu_z among those with mass diffusion, without mass diffusion, and previous experimental results (without mass diffusion) for $T_w = 40°C$ and $\phi = 50$ percent

balance out, and the local minimum Nusselt number appears at some downstream location. Subsequently, the free convection effect dominates over the entrance effect and the Nusselt number increases sharply. This indicates the initiation of a thermal and concentration-driven secondary flow, which becomes increasingly pronounced, until a maximum value for Nu_z is attained. The maximum is due to the secondary flow having developed over the entire spanwise field. This is the reason why the criterion based on the local minimum Nusselt number was chosen for comparison in this study. As shown in Figure 8, the solid lines illustrate that the results based on this criterion, under the thermal buoyancy effects only, for cases 1 and 4 have a good agreement with those of experimental work by Hwang and Liu[13] and Kamotani and Ostrach.[15] When the mass diffusion is considered in the flow, the predictions (shown by dashed lines in Figure 8) reveal an advanced onset point. Comparing the results shown in Figures 7a and 8, it is found that the predicted results based on the two criteria are different. In fact, the streamwise distance to the onset of instability based on the minimum Nusselt number (Figure 8) is certainly expected to be larger than that defined by a 2 percent departure (Figure 7a).

Concluding remarks

The onset of convective instability has been studied under the combined buoyancy effects of thermal and mass diffusion in the thermal entrance region of horizontal rectangular ducts. Two different instability criteria have been used to mark the onset point. The influences of the bottom wall temperature, relative humidity, and aspect ratio on the heat and mass transfer and instability are examined in substantial detail. What follows is a summary of the main results:

(1) The predicted results based on a 2 percent departure or the minimum of Nu_z show an advanced onset point compared with those without mass buoyancy effects.

(2) In the present study the system is more unstable for the system with higher bottom surface temperature T_w owing to the larger blowing effect (i.e., larger film evaporation rate), but the phenomenon is reversed for the higher relative humidity.

(3) Under fixed T_w and ϕ conditions, the results for large aspect ratio show a more stable situation than those for a small aspect ratio.

(4) Heat transfer along the wetted wall is dominated by the transport of latent heat associated with the vaporization of the liquid film.

(5) The variations of local Nu_z, Nu_s, and Sh_z are characterized by a decay near the channel inlet in which the forced convection entrance effect dominates, but the decay is attenuated by the onset of convecture instability, leading to a buoyancy-driven secondary flow. After a minimum has been reached, the values of Nu_z, Nu_s, and Sh_z increase and subsequently exhibit an oscillatory phenomenon when the effective Rayleigh number is sufficiently large.

Acknowledgment

The authors gratefully acknowledge the National Science Council of the Republic of China for the financial support of the present study through project NSC79-0401-E008-01.

References

1 Nakayama, W., Hwang, G. J. and Cheng, K. C. Thermal instability in plane Poiseuille flow. *ASME J. Heat Transfer*, 1970, **92**, 61–68

2 Hwang, G. J. and Cheng, K. C. Convective instability in the thermal entrance region of a horizontal parallel plate channel heated from below. *ASME J. Heat Transfer*, 1973, **95**, 72–77

3 Cheng, K. C. and Ou, J. W. Convective instability and finite amplitude convection in the thermal entrance region of horizontal rectangular channels heated from below. *Proc. 7th Int. Heat Transfer Conf.* Hemisphere, Washington, DC, 1982, **2**, 189–194

4 Cheng, K. C., Hong, S. W. and Hwang, G. J. Buoyancy effect on laminar heat transfer in the thermal entrance region of rectangular channels with uniform wall heat flux for large Prandtl number fluids. *Int. J. Heat Mass Transfer*, 1972, **17**, 1819–1836

5 Ou, J. W., Cheng, K. C. and Lin, R. C. Natural convection effect on Graetz problem in horizontal rectangular channels with uniform wall temperature for large Pr. *Int. J. Heat Mass Transfer*, 1974, **17**, 835–843

6 Abou-Ellail, M. M. M. and Morcos, S. M. Buoyancy effects in the entrance region of horizontal rectangular channels. *ASME J. Heat Transfer*, 1983, **105**, 924–928

7 Incropera, F. P. and Schutt, J. A. Numerical simulation of laminar mixed convection in the thermal entrance region of horizontal rectangular ducts. *Numer. Heat Transfer*, 1985, **8**, 707–729

8 Incropera, F. P., Knox, A. L. and Maughan, J. R. Mixed convection flow and heat transfer in the entry region of a horizontal rectangular duct. *ASME J. Heat Transfer*, 1987, **109**, 434–439

9 Mahaney, H. V., Incropera, F. P. and Ramadhyani, S. Development of laminar mixed convection in a horizontal rectangular duct with uniform bottom heating. *Numer. Heat Transfer*, 1987, **12**, 137–155

10 Chou, F. C. and Hwang, G. J. Vorticity-method for Graetz problem with the effect of natural convection in a horizontal rectangular channel with uniform wall heat flux. *ASME J. Heat Transfer*, 1987, **109**, 704–710

11 Lin, J. N., Chou, F. C. and Tzeng, P. Y. Theoretical prediction of the onset of thermal instability in the thermal entrance region of horizontal rectangular channels. *Int. J. Heat Fluid Flow*, 1991, **12**, 218–224

12 Akiyama, M., Hwang, G. J. and Cheng, K. C. Experiments on the onset of longitudinal vortices in laminar forced convection between horizontal plates. *ASME J. Heat Transfer*, 1971, **93**, 335–341

13 Hwang, G. J. and Liu, C. L. An experimental study of convective instability in the thermal entrance region of a horizontal parallel-plate channel heated from below. *Can. J. Chem. Eng.*, 1976, **54**, 521–525

14 Kamotani, Y., Ostrach, S. and Miao, H. Convective heat transfer augmentation by means of thermal instability. *ASME J. Heat Transfer*, 1979, **101**, 222–226

15 Kamotani, Y. and Ostrach, S. Effect of thermal instability on thermally developing laminar channel flow. *ASME J. Heat Transfer*, 1976, **98**, 62–66

16 Incropera, P., Knox, A. L. and Schutt, J. A. Onset of thermally driven secondary flow in horizontal rectangular ducts. *Proc. 8th Int. Heat Transfer Conf.* Hemisphere, Washington, DC, 1986, **3**, 1395–1400

17 Sound-Algeker, V. M. and Ganesan, P. Finite difference analysis of transient free convection with mass transfer on an isothermal vertical flat plate. *Int. J. Eng. Sci.*, 1981, **19**, 757–770

18 Lee, T. S., Parikh, P. G., Acrivos, A. and Bershader, D. Natural convection in a vertical channel with opposing buoyancy forces. *Int. J. Heat Mass Transfer*, 1982, **25**, 499–511

19 Chang, C. J., Lin, T. F. and Yan, W. M. Natural convection flows in a vertical open tube resulting from combined buoyancy effects of thermal and mass diffusion. *Int. J. Heat Mass Transfer*, 1986, **29**, 1543–1552

20 Santarelli, F. and Foraboschi, F. P. Heat transfer in laminar mixed convection in a reacting fluid. *Chem. Eng.*, 1973, **6**, 59–68

21 Lin, T. F., Chang, C. J. and Yan, W. M. Analysis of combined buoyancy effects of thermal and mass diffusion on laminar forced convection heat transfer in a vertical tube. *ASME J. Heat Transfer*, 1988, **110**, 337–367

22 Yan, W. M., Tsay, Y. L. and Lin, T. F. Simultaneous heat and mass transfer in laminar mixed convection flow between vertical parallel plates with asymmetric heating. *Int. J. Heat Fluid Flow*, 1989, **10**, 262–269

23 Yan, W. M. and Lin, T. F. Natural convection heat and mass transfer between vertical parallel plates with film evaporation. *Int. J. Heat Mass Transfer*, 1990, **33**, 529–541

24 Chow, L. C. and Chung, J. N. Evaporation of water into a laminar stream of air and superheated stream. *Int. J. Heat Mass Transfer*, 1983, **26**, 373–380

25 Fujii, T., Kato, Y. and Mihara, K. Expressions of transport and thermodynamic properties of air, steam and water. Sei. San Ka Gaku Ken Kyu Jo, Report no. 66, Kyu Shu Dai Gaku, Kyu Shu, Japan, 1977, 81–95

26 Yan, W. M. Boundary induced heat and mass transfer in vertical channel flows. Ph.D. thesis, Department of Mechanical Engineering, National Chiao Tung University, Hsinchu, Taiwan, 1989

27 Burmeister, L. C. *Convective Heat Transfer*, 2nd ed. McGraw-Hill, New York, 1983, 170–174

28 Eckert, E. R. G. and Drake, Jr, R. M. *Analysis of Heat and Mass Transfer*, 1st ed. McGraw-Hill, New York, 1972, 715–759

29 Ou, J. W. and Cheng, K. C. Natural convection effects on Graetz problem in horizontal isothermal tubes. *Int. J. Heat Mass Transfer*, 1977, **20**, 953–960